Plasma response to m/n = 3/1 resonant magnetic perturbation on J-TEXT Tokamak

Qiming Hu[1], Jianchao Li[1], Nengchao Wang[1], Q. Yu[2, 3], Jie Chen[1], Zhifeng Cheng[1], Zhipeng Chen[1], Yonghua Ding[1], Hai Jin[1], Da Li[1], Mao Li[1], Yang Liu[1], Bo Rao[1], Lizhi Zhu[1], Ge Zhuang[1] and the J-TEXT Team

[1] *State Key Laboratory of Advanced Electromagnetic Engineering and Technology, School of Electric and Electronic Engineering, HuazhongUniversity of Science and Technology, 430074, Wuhan, China*

[2] *Max-Planck-Institut für Plasmaphysik, 85748 Garching, Germany*

Email: qiy@ipp.mpg.de

Abstract The influence of resonant magnetic perturbations (RMPs) with a large $m/n = 3/1$ component on electron density has been studied on J-TEXT tokamak by using externally applied static and rotating RMPs, where m and n are the poloidal and toroidal mode number, respectively. The detailed time evolution of electron density profile, measured by the polarimeter-interferometer, shows that the electron density n_e first increases (decreases) inside (around/outside) of the 3/1 rational surface (RS), and it is increased globally later together with enhanced edge recycling. Associated with field penetration, the toroidal rotation around the 3/1 RS is accelerated in co-I_p direction and the poloidal rotation is changed from electron to ion diamagnetic drift direction. Spontaneous unlocking-penetration circles occur after field penetration if the RMPs amplitude is not strong enough. While for sufficiently strong RMPs, the 2/1 locked mode is also triggered due to mode coupling, and the global density is increased. The field penetration threshold is found to be linearly proportional to the n_eL (line-integrated density) at the 3/1 RS but to $(n_e L)^{0.73}$ for the n_e at plasma core. In addition, for rotating RMPs with a large 3/1 component, field penetration causes global increase in electron density.

1. Introduction

Resonant magnetic perturbations (RMPs) generated by external saddle coils have important applications in present tokamak plasmas. RMPs have been demonstrated firstly on DIII-D to be a promising technique in mitigating/suppressing edge localized modes (ELMs) [1, 2], and subsequently ELMs control by RMPs were also investigated on JET [3], ASDEX-Upgrade [4], KATAR [5], MAST [6] and other tokamaks. RMPs have also been used to detect and correct the non-axisymmetric error field arising from misshapen or misplaced coils and their leads [7, 8], and many corresponding studies have been carried out on DIII-D [9-11], MAST [12] and KSTAR [13]. In addition, RMPs have also been used in active stabilization of resistive wall modes (RWMs) [14-16].

It is well known phenomena that the application of RMPs to mitigate ELMs or correct error field often leads to the change in the electron density, the so-called density pump-out [1-3, 17]. This change affects the L-H transition power [18-20] and fusion gain in the future burning plasmas. For the extrapolation of the application of RMPs to future devices with minimum degradation on particle and thermal confinement as well as minimum effects on L-H transition and MHD instabilities, it is important to understand the effects of RMPs on particle transport in both the L- and H-mode plasmas.

The particle transport in the presence of RMPs has been extensively studied before. In L-mode plasmas, the density pump-out caused by applied RMPs is found to behave as a resonant feature, as observed on TEXTOR [21, 22] and LHD [23]. Depending on the RMPs spectrum as well as the

[3] Authors to whom any correspondence should be addressed.

plasma parameters, either an improvement or a decrease in particle confinement is observed on Tore-Supra [24] and TEXTOR [22, 25, 26], and these experimental results can be reproduced by numerical modeling [27, 28]. On MAST the density pump-out is exhibited only when the RMP coil current is above a threshold, and the radial electric field E_r is also changed in a layer just inside the separatrix [29]. Comparisons on the change in the plasma density and rotation reveal that E_r is changed due to the modification of the toroidal/poloidal rotation, which might affects the particle transport [25, 29]. In addition, RMPs are found to cause the particle pinch to reverse from traditionally inward to outward, and the density at the plasma edge increases, while the density in the plasma core is reduced as observed on DIII-D [20]. For H-mode plasmas, it is observed that the density pump-out depends on the collisionality [30]. Studies carried out on DIII-D show that both the toroidal rotation and E_r are modified when density pump-out occurs [20], and the outward diffusion increases with application of RMPs whereas the inward pinch decreases [31]. To understand the physics basis of this topic, further studies on different devices are necessary.

Previous studies on J-TEXT exhibit resonant feature for the influence of RMPs on particle transport, and density pump-out occurs when $m/n = 2/1$ locked mode is triggered by the 2/1 RMP [32], where m and n are the poloidal and toroidal mode number, respectively. Recent studies by using rotating 2/1 RMPs showed that RMPs improve (degrade) particle confinement when its frequency is higher (lower) than the natural 2/1 tearing mode (TM) frequency, and the amount of change in electron density is proportional to the difference between these two frequencies [33], being in good agreement with numerical predictions [27, 28].

In this paper, we focus on the plasma response to both static and rotating RMPs with its resonant position close to the plasma edge. In the experiment, the saddle coils is connected to generate a large 3/1 component, and the edge safety factor is chosen to be around 3.3. As a result, the field penetration of the 3/1 RMP is observed. The time evolution of the radial profile of electron density is measured by the multi-channel polarimeter-interferometer (POLARIS). For static RMPs, after field penetration the density is increased (decreased) inside (around/outside) the 3/1 RS firstly, and the global density is increased later. The toroidal rotation around the 3/1 RS is accelerated in co-I_p direction and the poloidal rotation is changed from electron to ion diamagnetic drift direction. The change in electron density causes spontaneous unlocking-penetration circles, and the 2/1 locked mode is also excited when the RMPs are strong enough. In addition, the scaling of penetration threshold on electron density is also studied. For rotating RMPs, field penetration causes an increase in global density. In Section 2 the experimental results are given: the experimental setup is described in section 2.1; the influence of static RMPs on density and the associated change in rotation are then presented in sections 2.2 and 2.3; in section 2.4 the results obtained by rotating RMPs are presented. Finally, discussions and summary are drawn in Section 3.

2. Experimental setup and results

2.1. Experimental setup

J-TEXT is a circular, medium sized, limiter tokamak with a major radius (R_0) of 1.05 m and a minor radius (a) of 0.25-0.3 m [34]. Recently, J-TEXT had been equipped with 12 in-vessel saddle coils, which can generate either static or rotating RMPs with a maximum frequency up to 6 kHz [35]. In the present experiments, the connection of coil system is set to produce RMPs with a large $m/n = 3/1$ resonant component. The spectrum of static RMPs calculated in vacuum condition is shown in figure 1(a), which is dominated by the $m/n = 1/1$ and 3/1 components for edge safety factor $q_a > 3$. The 3/1 component at the plasma edge is $b_r^{3,1}(r = a) = 1.2$ Gs/kA. Rotating RMPs are generated when the coil system is supplied with AC current, and the field spectrum calculated for

the frequency of 5.3 kHz is shown in figure 1(b). The eddy current in the vacuum vessel decreases the field amplitude of 3/1 component to about 0.29 Gs/kA at plasma edge for f_{RMP} = 5.3 kHz.
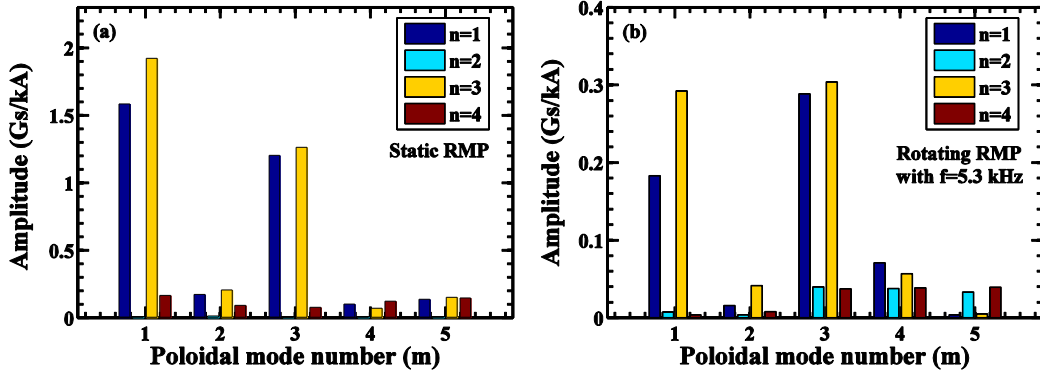

Figure 1. Spectrum of the radial magnetic field b_r generated by the saddle coils for (a) static RMPs and (b) rotating RMPs of a frequency f_{RMP} = 5.3 kHz at the plasma edge ($r = a$) with poloidal mode number (m) in the range of 1-5 and toroidal mode number (n) in the range of 1-4. The magnetic field is calculated with vacuum condition, and the eddy current in the vacuum vessel is taken into account for calculating the spectrum of rotating RMPs with f_{RMP} = 5.3 kHz.
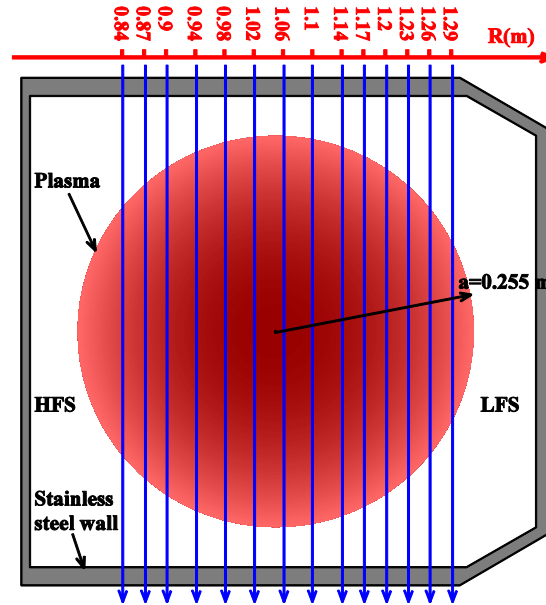

Figure 2. Diagram of multi-channel polarimeter-interferometer (POLARIS) for electron density measurement, which views the plasma vertically, and the radial positions are shown.

In the experiment, the electron density is measured by multi-channel polarimeter-interferometer (POLARIS) [36], which views the plasma vertically by 14 channels with the impact positions ranging from R = 0.84 m to 1.29 m as shown in figure 2, and the spatial temporal resolution are 30 mm and 1 μs. The electron density provided by the channel at/around R = 1.05 m is used to interpret the experimental results in the context. It will be noted in the text where the line-integrated density instead of line-averaged density is used. The MHD activity is measured by both the poloidal and toroidal probe arrays, where the poloidal array consists of 24 probes evenly distributed in poloidal direction. The locked mode detectors consist of two sets of saddle loops. Each set contains two loops installed at two opposite toroidal locations outside of the vacuum vessel [37]. The difference between the signals from two saddle loops in one set shows the perturbation with odd toroidal mode number (n = 1, 3, 5, ...). The electron temperature is measured by an 8-channel heterodyne electron cyclotron emission (ECE) radiometer [38]. The toroidal and poloidal rotation of carbon V (CV) and carbon III (CIII) impurity at the edge of low field side are measured by a multi-channel high resolution spectrometer [39].

2.2. Experimental results with static RMPs

For the experimental results described in this subsection, the plasma parameters are as follows unless otherwise noted: major/minor radius (R_0/a) is 1.05 m/0.255 m, plasma current I_p = 160 kA, toroidal magnetic field B_t = 1.65 T, and the safety factor q = 3.3 at the plasma edge. The core line-integrated electron density at R = 1.05m is around 0.3-0.8 $\times 10^{19}$m^{-2}. The central plasma rotation is observed to be in the *electron diamagnetic drift direction*, and the plasma is originally tearing stable.
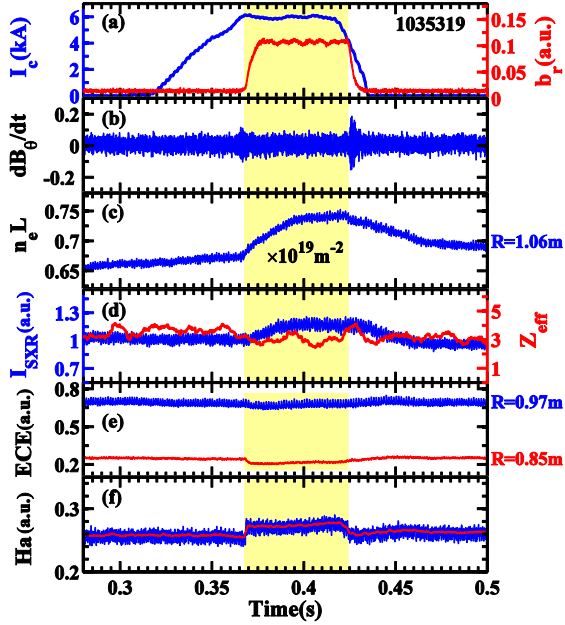
Figure 3. Shot 1035319, penetration of static 3/1 RMPs. Time evolution of (a) I_c and b_r, (b) Mirnov signal dB_θ/dt, (c) core integrated density n_eL, (d) core SXR radiation intensity I_{SXR} and Z_{eff}, (e) ECE signal at R = 0.97 m and 0.85 m, and (f) edge Hα signal.

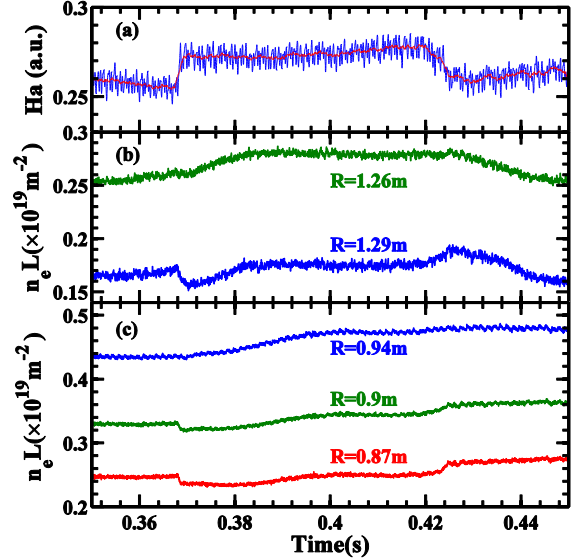**Figure 4.** Corresponding to figure 3, time evolution of (a) Ha signal, integrated electron density at (b) LFS (R = 1.26 m and 1.29 m) and (c) HFS (R = 0.87 m, 0.9 m, and 0.94 m).

An example of the effect of static 3/1 RMPs on the electron density during field penetration is shown in figure 3 for shot 1035319. Before the application of RMPs, the plasma parameters nearly keep constant. The RMP coil current (I_c) is applied at 0.32 s (figure 3(a)), and it ramps up to the flattop of 6 kA at 0.36 s. Field penetration happens at t = 0.368 s as indicated by the fast growth of the locked mode detector signal b_r (red curve in figure 3(a)) when I_c ramps up to 5.9 kA. After field penetration, the line-integrated electron density n_eL at R = 1.06 m begins to increase from 0.67 $\times$ 10^{19} m^{-2} to 0.75 $\times$ 10^{19} m^{-2} (figure 3(b)), with a relative change of 12%. At the same time, the electron temperature decreases slightly close to plasma core (R = 0.97 m) and more obvious at plasma edge (R = 0.85 m) as shown in figure 3(d). The soft X-ray emission (SXR) at plasma core increases and the effective Z_{eff} is slightly decreased (figure 3(c)). The edge recycling increases slightly as indicated by the Hα signal at r = 0.27 m. At t = 0.425 s mode unlocking happens when I_c ramps down to 4 kA, and all the parameters begin to recover to their initial values. The unlocking threshold is only one third smaller than the penetration threshold, being smaller than that for the 2/1 and other modes as reported on COMPASS [40], J-TEXT [41, 42] and EXTRAP-T2R [43]. The possible reason for this is the change in plasma rotation, which will be discussed in section 2.3.

In figure 4, the time evolution of n_eL around the 3/1 RS at both LFS and HFS are shown. For shot 1035319 the 3/1 RS is found to be around R = 1.27 m at LFS and 0.9 m at HFS. It is found that n_eL first decreases quickly around/outside of the 3/1 RS (for R = 1.29 m at LFS and $R \leq$ 0.9 m at HFS) right after field penetration. Afterwards the n_eL increases both outside and inside the 3/1 RS.
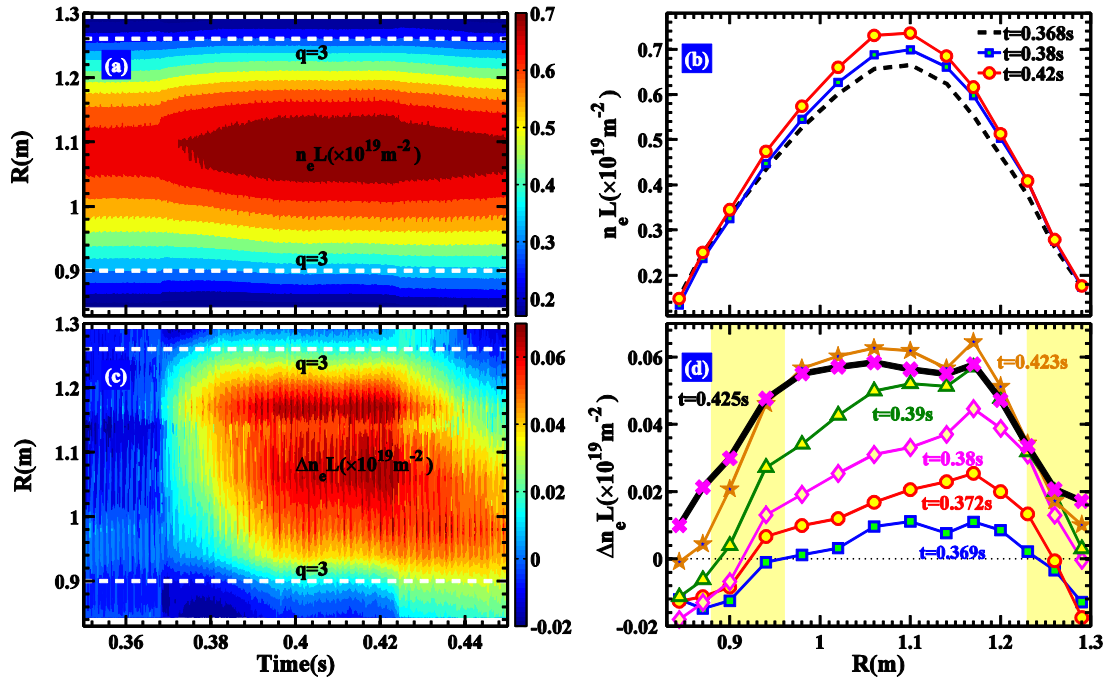
Figure 5. Corresponding to figure 3, time evolution of profile of n_eL (a) in the interval of 0.35 s < t < 0.45 s and (b) at t = 0.368 s, 0.38 s, and 0.42 s. Time evolution of profile of $\Delta n_eL = (n_eL-n_eL(t = 0.368\,s))$ (c) in the interval of 0.35 s < t < 0.45 s and (d) at t = 0.369 s, 0.372 s, 0.38 s, 0.39 s, 0.423 s, and 0.425 s.

The time evolution of the profile of n_eL and the changed density $\Delta n_eL = [(n_eL(t) - n_eL(t = 0.368s)]$ are shown in figure 5(a)-5(d). During the field penetration, n_eL first increases inside the 3/1 RS but decreases around/outside of the 3/1 RS (figure 5(a) and 5(c)), and then the global density is raised as indicated by the profile of n_eL at t = 0.38 s and 0.42 s before mode unlocking as shown in figure 5(b). The profiles of Δn_eL at different times show that the gradient of density around the 3/1 RS is stronger (marked by the shadowed region in figure 5(d)), and it changes little during the raise of the profile. In addition, after mode unlocking, the profile of Δn_eL at t = 0.425 s decreases little at plasma core but increases at plasma edge, and afterwards Δn_eL declines with time. Results shown in figures 3 to 5 indicate that the penetration of the 3/1 RMP first increases (decreases) electron density inside (around/outside of) the 3/1 RS and then increases the global electron density. The electron temperature decreases slightly except a stronger reduction at plasma edge, and the edge recycling is slightly increased.
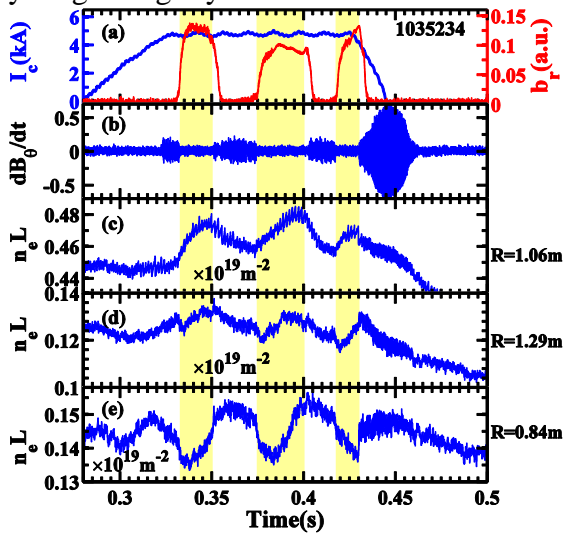

Figure 6. Shot 1035234, penetration of static 3/1 RMPs. Time evolution of I_c, b_r, dB_θ/dt, integrated density n_eL at R = 1.06 m, 1.29 m and 0.87 m.
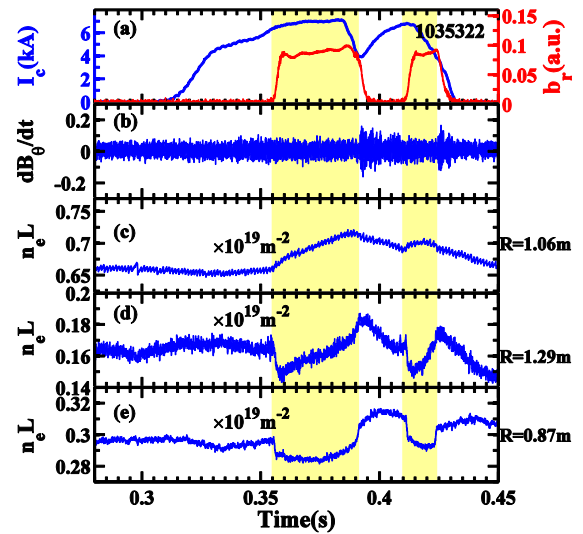
Figure 7. Shot 1035322, penetration of static 3/1 RMPs. Time evolution of I_c, b_r, dB_θ/dt, integrated density n_eL at R = 1.06 m, 1.29 m and 0.87 m.

After field penetration, the increased density may exceed the density threshold for penetration

and then force the locked mode to unlock when the amplitude of RMPs is not strong enough. One typical result is shown in figure 6 for shot 1035234, here I_c = 4.7 kA at the flattop and n_eL is 0.45×10^{19} m^{-2} before penetration. After field penetration at t = 0.33 s, edge n_eL decreases (at R = 1.29 m and 0.84m) firstly, and later on it increases accompanying with the increase of central density (n_eL at R = 1.06 m). At t = 0.35 s, the central density increases to n_eL = 0.48×10^{19} m^{-2} and the edge density exceeds the density threshold for penetration, so that mode unlocking happens spontaneously. The global density decreases after mode unlocking, which is similar to the result as shown in figure 5. When the density decreases to the value near the density threshold, field penetration happens again at t = 0.365 s and 0.42 s, respectively. When first decreasing and then increasing I_c after field penetration, the penetration-unlocking circle is also observed as shown in figure 7 for shot 1035322.
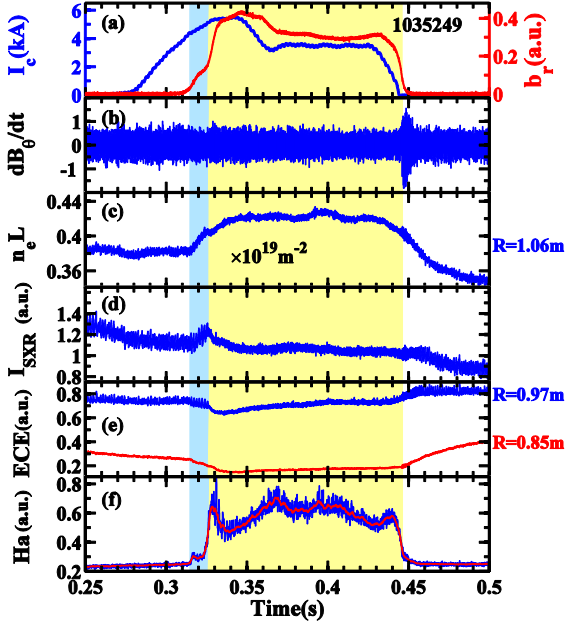

Figure 8. Shot 1035249, penetration of static 3/1 RMPs and excitation of 2/1 locked mode. Time evolution of I_c, b_r, dB_θ/dt, n_eL at plasma core, core SXR radiation intensity I_{SXR}, ECE signal at R = 0.97 m and 0.85 m, and edge Hα signal.
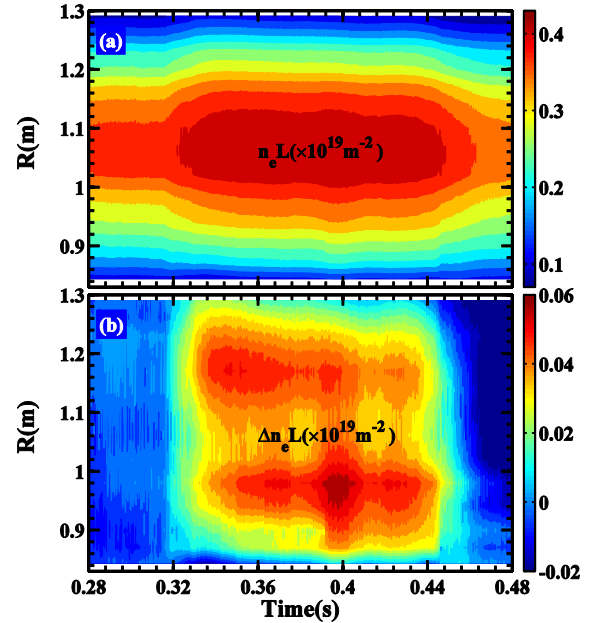
Figure 9. Corresponding to figure 8, time evolution of profile of (a) n_eL and (b) Δn_eL = (n_eL - $n_eL(t = 0.28$ s)) in the interval of 0.28 s < t < 0.48 s.

For the plasma with lower equilibrium density, the 3/1 locked mode together with a weak 2/1 component of RMPs may trigger an additional 2/1 locked mode when the applied RMPs are strong enough relative to penetration threshold, as shown in figure 8 for shot 1035249. Here, I_c = 5.5 kA at the first flattop and n_eL = 0.37×10^{19} m^{-2}. During the time interval of 0.315 s < t < 0.325 s, a 3/1 locked mode is triggered and the changes in all measured signals are similar to those shown in figure 3. However, for 0.325 s < t < 0.445 s, the b_r signal, the n_eL at plasma core and the Hα signal further increase to a higher level (figure 8(a), (b), (e)), while the electron temperature at both plasma core and edge decrease substantially, and the SXR signal decreases slightly. By analyzing the Mirnov signal right after mode unlocking, it is found that both the 2/1 and the 3/1 modes exist, indicating that a 2/1 locked mode is also triggered after the field penetration of 3/1 RMPs. Differing from the usual occurrence of 2/1 locked mode with density pump-out [32, 44], in figure 8 the plasma density increases after the trigger of 2/1 locked mode. Corresponding to figure 8, the time evolution of the radial profile of n_eL and Δn_eL = (n_eL - $n_eL(t = 0.28$ s)) are shown in figure 9(a) and 9(b), respectively. It is found that, the global density is increased except the slight reduction at the very edge of HFS during the interval of 0.325 s < t < 0.35 s. Besides, the profile of Δn_eL peaks at R = 1.18 m and 0.96 m of LFS and HFS, revealing that stronger density gradient is formed outside both the radius. Further experiments reveal that the phenomena shown in figures 8 and 9 are repeatable, and the increased density can be maintained with a lower I_c after field penetration as

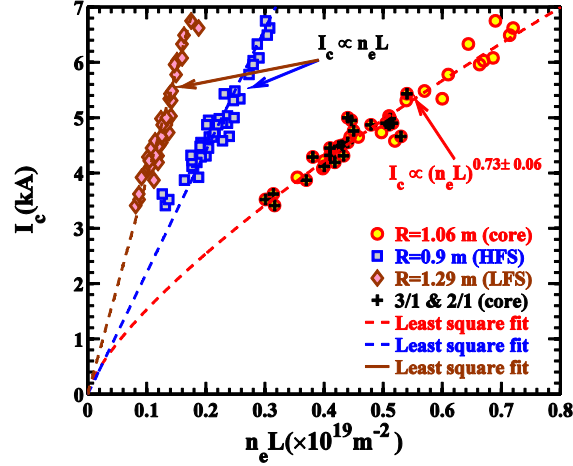shown in figure 8(a), but disruption may happen later if I_c has not been lowered down from the flattop.

Figure 10. Data obtained from density scanning discharges with fixed plasma current I_p= 160 kA, toroidal field B_t=1.65 T and q_a=3.3, showing the line-integrated electron density n_eL versus the amplitude of RMP coil current I_c. The red circles (○) represent the penetration threshold of n_eL at R = 1.06 m, the blue squares (□) and brown diamonds (◊) represent the penetration threshold of n_eL at R = 0.87 m and 1.29 m. The pluses (+) represent the shots that 2/1 locked mode is excited. The dashed curves are obtained from the least-squares fit for the penetration cases using a power law, and the obtained density scaling is $I_c \propto (n_eL)^{0.73\pm0.06}$ at R = 1.06 m and $I_c \propto n_eL$ at R = 0.89 m.

The relationship between the penetration threshold and the electron density is investigated by scanning the central n_eL from 0.3×10^{19} m^{-2} to 0.75×10^{19} m^{-2}. The RMPs coil current I_c at the moment of field penetration is taken to be the penetration threshold. The relationship between the penetration threshold and the n_eL at different radius is shown in figure 10. The red circles (○) represent the penetration threshold for the n_eL at R = 1.06 m, and the blue squares (□) and brown diamonds (◊) represent the penetration threshold for the n_eL at R = 0.9 m and 1.29 m. Here, the radial positions of R = 0.9 m and 1.29 m are the closest chords outside of the 3/1 RS on the HFS and LFS. The pluses (+) represent the shots that the 2/1 locked mode is also excited after the field penetration of the 3/1 RMP. The corresponding electron density is measured at the moment of penetration. It is found that the penetration threshold increases with the density. The least-squares fit for the penetration data using a power law is marked by the dashed curves and displays a density scaling of $I_c \propto (n_eL)^{0.73\pm0.06}$ for the central density at R = 1.06 m, and $I_c \propto n_eL$ for the edge density at R = 0.9 m and 1.29 m (around 3/1 RS). These results are different from the scaling of penetration threshold for 2/1 mode on other tokamaks, which usually scale in linear for the central density [45-47]. Another scaling $I_c \propto n_e^{0.5}$ is also found on TEXTOR [48] and J-TEXT [49].

2.3. Change in plasma rotation

Previous studies on TEXTOR show that the change in electron density correlates with the change in plasma rotation and E_r [25], and numerical modeling also finds that, depending on the direction of plasma rotation, the density can be either increased or decreased [27, 28]. During the experiment with static RMPs, both the toroidal and poloidal rotation of CV and CIII have been measured, and CV and CIII cover the region of 0.75-0.85 a and 0.85-0.95 a (around the 3/1 RS at LFS), respectively. Corresponding to figure 6, the time evolution of both the toroidal and poloidal rotation of CV and CIII are shown in figure 11. Here, the positive value indicates the co-I_p direction or the ion diamagnetic drift direction for toroidal and poloidal rotation, respectively. It is found that V_ϕ(CV) changes from 0 to nearly 4 km/s, while V_ϕ(CIII) changes little. The poloidal rotation velocity V_θ(CV) increases slightly and V_θ(CIII) increases from -1.5 km/s to 1 km/s in ion diamagnetic drift direction (f_{*ion}). After mode unlocking, all the rotation velocities recover to their initial values.
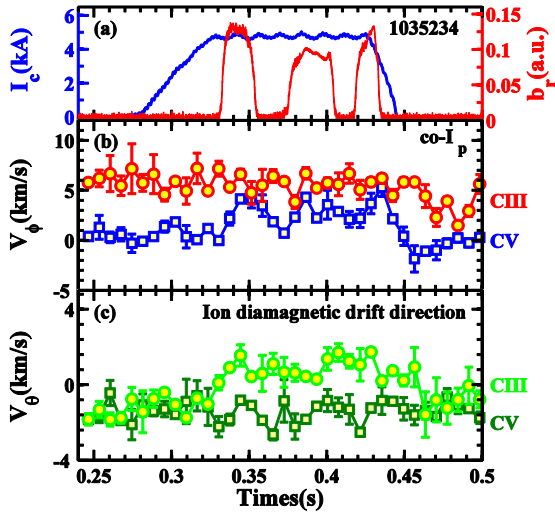
Figure 11. Corresponding to figure 6, the time evolution of (a) I_c and b_r, (b) toroidal rotation of CV (squares) and CIII (circles) and (c) poloidal rotation of CV (squares) and CIII (circles).

Figure 12. Corresponding to figure 8, the time evolution of (a) I_c and b_r, (b) toroidal rotation of CV (squares) and CIII (circles) and (c) poloidal rotation of CV (squares) and CIII (circles).
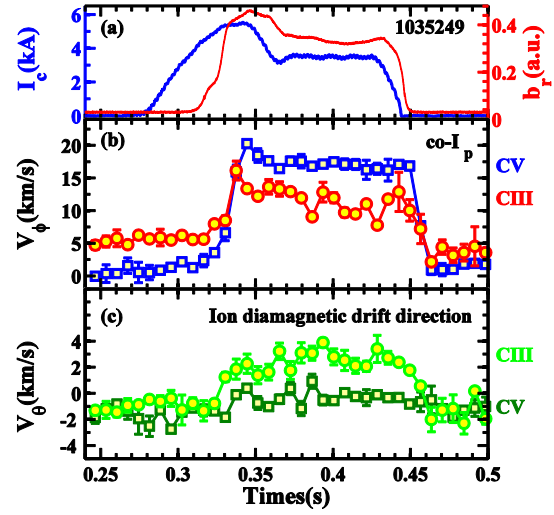
When the amplitude of RMPs is strong enough and a 2/1 locked mode is excited, the change in rotation is similar to that shown in figure 11. Corresponding to figure 8, the time evolution of both the V_ϕ and V_θ of CV and CIII are shown in figure 12. It is found that $V_\phi(CV)$ and $V_\phi(CIII)$ are increased to 17.5 km/s and 11.2 km/s in the co-I_p direction, respectively, which is similar to the results of field penetration and mode locking observed on COMPASS [40] and J-TEXT [50]. For poloidal rotation, $V_\theta(CV)$ and $V_\theta(CIII)$ increases from -2 km/s to 0 and -1.5 km/s to 3 km/s in co-f_{*ion} direction.
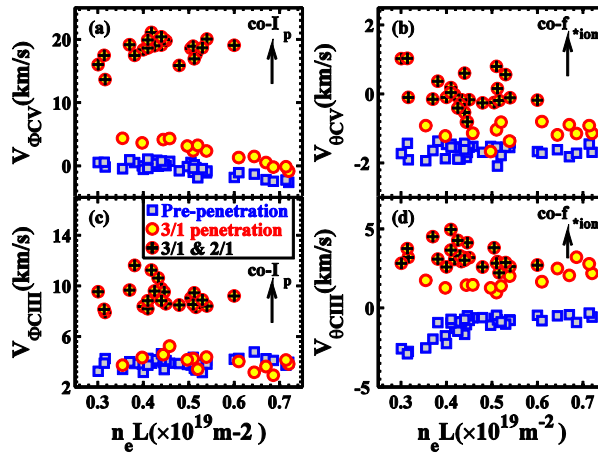

Figure 13. Corresponding to figure 10, the toroidal and poloidal rotation before (squares) and after (circles) field penetration are shown as a function of core line-integrated density n_eL. (a) V_ϕ and (b) V_θ of CV, (c) V_ϕ and (d) V_θ of CIII.

Corresponding to figure 10, the toroidal and poloidal rotation before and after field penetration are shown as a function of core line-integrated density in figure 13. It is found that before the penetration of RMPs, V_ϕ and V_θ decrease slightly towards counter-I_p and the electron diamagnetic drift direction respectively with increasing the electron density. The penetration of 3/1 RMPs causes a increase of ~ 4 km/s in the co-I_p direction for $V_\phi(CV)$, while $V_\phi(CIII)$ changes little. $V_\theta(CV)$ and $V_\theta(CIII)$ increase by about 1 km/s and 3 km/s towards co-I_p and ion diamagnetic drift direction. When a 2/1 locked mode is further excited, $V_\phi(CV)$ and $V_\phi(CIII)$ are substantially accelerated in the co-I_p direction, while $V_\theta(CV)$ and $V_\theta(CIII)$ are accelerated in ion diamagnetic drift direction. By comparing to the results in section 2.2 and in figure 12, a correlation between the change in density and rotation is found: associated with the increased electron density, the poloidal rotation around the 3/1 RS is accelerated to co-f_{*ion} direction, while the rotation inside the 3/1 RS changes little. And

this correlation is consistent with the numerical prediction [27, 28] and experimental observations [33]. In addition, the plasma rotation around 3/1 RS is low and the change in rotation is moderate after field penetration, resulting in that the mode unlocking occurs easily when ramping down RMP current, as shown in figures 3 and 6.

2.4. Experimental results with rotating RMPs

Similar to the results presented in section 2.2, rotating RMP is also applied to study the change in electron density and it rotates in the counter-I_p (electron diamagnetic drift) direction. In the experiments, the plasma parameters are as follows: major/minor radius (R_0/a) is 1.05 m/0.255 m, plasma current $I_p = 160$ kA, toroidal magnetic field $B_t = 1.55$ T, and the safety factor $q_a = 3.14$ at the plasma edge. The core line-integrated electron density at $R = 1.05$m is around 0.4-0.5$\times 10^{19}$m^{-2}.
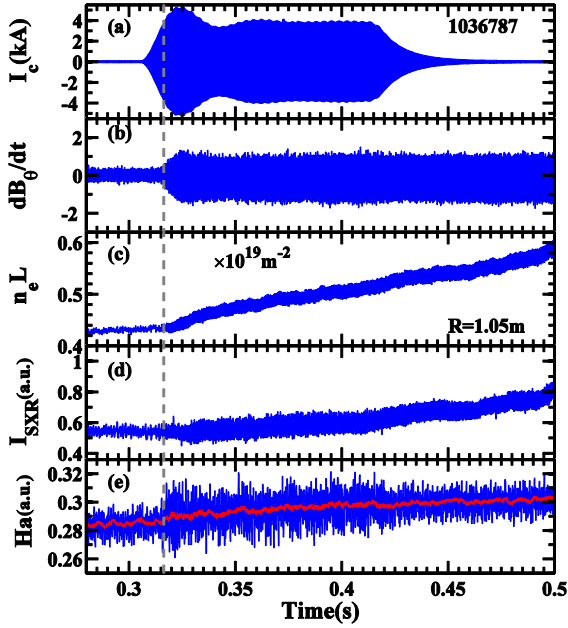

Figure 14. Shot 1036787, field penetration of rotating 3/1 RMPs with $f_{RMP} = 5.3$ kHz. Time evolution of I_c, dB_θ/dt, n_eL at $R = 1.05$ m, core SXR radiation intensity I_{SXR}, and edge Hα signal.
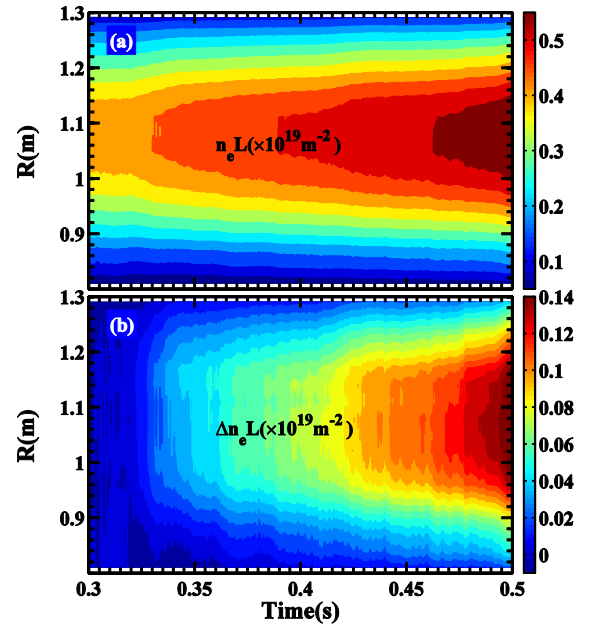
Figure 15. Corresponding to figure 14, time evolution of the radial profile of (a) n_eL and (b) the changed density $\Delta n_eL = (n_eL - n_eL(t = 0.32$ s$))$ in the interval of 0.3 s $< t <$ 0.5 s.

An example of the effect of rotating RMPs on electron density is shown in figure 14 with the rotating frequency of $f_{RMP} = 5.3$ kHz and $I_c = 4$ kA at the flattop. Before applying RMPs, the plasma is tearing stable and the parameters keep constant. At $t = 0.305$ s, rotating RMPs are turned on, field penetration happens later at t = 0.315 s when I_c ramps up to 3.1 kA (figure 14(b)), so that a rotating 3/1 TM is triggered and driven to rotate synchronously with RMPs at 5.3 kHz. And this 3/1 rotating TM does not vanish after turning off RMPs at $t = 0.42$s, having a frequency 4 kHz. After field penetration, the line-integrated electron density n_eL at $R = 1.05$ m increases from 0.43 to 0.6 $\times 10^{19}$ m^{-2}, with a relative change of 40%. The density fluctuation correlated with rotating 3/1 TM is observed (figure 14 (c)). The time evolution of the radial profile of n_eL and the relative (to that at $t = 0.32$) density change Δn_eL as shown in figure 15(a) and 15(b) indicates that the global density is increased, and no opposite change in density is observed around the 3/1 RS. The SXR signal increases continuously associated with the increase of density (figure 14(d)), and the edge recycling increases slightly as indicated by the Hα signal at $r = 0.27$ m (figure 14(e)). Results shown in figures 14 and 15 indicate that the field penetration of 3/1 rotating RMPs increases the electron density in this case, and such an increase happens globally.
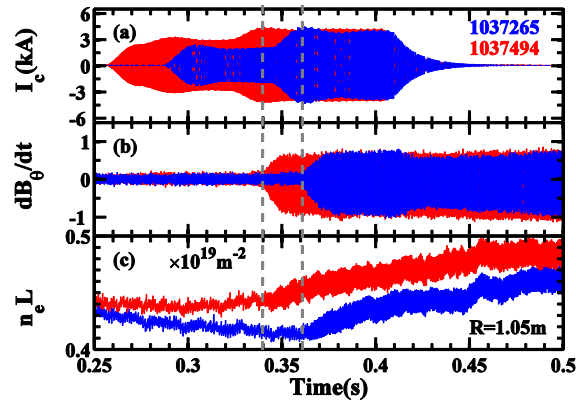
Figure 16. Shot 1037265 and 1037494, field penetration of rotating 3/1 RMPs. Time evolution of I_c, dB_θ/dt, and line-integrated density n_eL at $R = 1.05$ m.

In order to study the effect of rotating RMPs amplitude on the change of electron density, the waveform of I_c is controlled to ramp up with two flattops as shown in figure 16. For shot 1037265, I_c is set to ramp up to 2 kA and keeps 50 ms at the first flattop with field penetration. It is found that the rotating RMPs have no effect on electron density and edge recycling. Here the decrease in n_eL is mainly due to the decreasing gas puffing fueling. At $t = 0.36$ s, when I_c further ramps up to 4 kA at the second flattop, field penetration happens and n_eL begins to increase. For shot 1037494, I_c is set to ramp up to 3 kA at the first flattop and 4 kA at the second flattop, and similar results to shot 1037265 are observed when field penetration happens. For both the shots, the global density is increased after field penetration. Additional studies have also been carried out to look into the effect of the rotating frequency of RMPs, it is found that field penetration happens only when f_{RMP} is high enough (5.3 and 6.4 kHz) with maximum I_c.

3. Discussion and summary

By using both static and rotating RMPs with a large 3/1 component, the RMP effect on electron density have been studied on J-TEXT tokamak in the conditions of edge safety factor $q_a \sim 3.2\text{-}3.3$ with core plasma rotating in the *electron diamagnetic drift direction*. For tearing-stable plasmas, the detailed time evolution of density profile shows that the n_eL increases (decreases) inside (around/outside of) the 3/1 RS at first, and the global density is increased later. After field penetration, spontaneous unlocking-penetration circles occur due to the changed density when the RMP amplitude is not strong enough. While for strong enough RMPs, the 2/1 locked mode is also excited, and the global density is further increased. The coil current required for field penetration increases with the electron density, and it is proportionally to the n_eL at the 3/1 RS but to $(n_eL)^{0.73}$ for the density at plasma core. The penetration of 3/1 RMPs causes an increase of ~ 4 km/s for V_ϕ(CV) in the co-I_p direction, little change in V_ϕ(CIII), and an increase of 1 km/s and 3 km/s for V_θ(CV) and V_θ(CIII) towards ion diamagnetic drift direction. In addition, for rotating RMPs with a large 3/1 component, field penetration causes global increase in electron density.

Regarding the effect of RMPs on electron density, the fast decrease of the electron density right after field penetration, as shown in figures 4 and 5, seems to be consistent with the two fluid theory [27], since the plasma rotation is along the electron drift direction. However, the mechanism for the fast increase in the central electron density right after field penetration has not been identified yet. It is possible due to the change of plasma turbulence level in the central region, since plasma rotation is changed by the RMP. The applied RMPs are shown to be able to change the turbulence transport [31,51-54]. The global increase of the electron density well after the field penetration might also be associated the enhanced edge recycling. For rotating RMPs with a large 3/1 component, the increased electron density is consistent with previous finding that a sufficiently high rotating

frequency of RMPs increases the electron density [33], but the enhanced edge recycling might also play a role here.

Previous nonlinear numerical calculations based two-fluids equations reveal that with increasing the RMP amplitude, the local plasma rotation frequency is forced to approach the local electron diamagnetic drift frequency and to rotate towards the ion drift direction [55], providing a possible explanation for the plasma rotation acceleration by DED observed on TEXTOR [26]. For the experimental results with static 3/1 RMP presented in this paper, the increased electron density results in a stronger density gradient and hence a larger electron diamagnetic drift frequency around the 3/1 RS. According to the results in [55], the plasma will be forced to rotate towards the ion diamagnetic drift direction in order to make the total rotation speed of electron fluid to be zero, being consistent with the experimental results as presented in section 2.3.

In summary, the influence of both static and rotating RMPs on the change of electron density has been studied on J-TEXT Ohmic plasmas. The major results are as follows:

(1) Electron density first increases (decreases) inside (around/outside of) the 3/1 RS right after field penetration, and the global density is increased later associated with increased edge recycling.

(2) For static RMPs, after field penetration either unlocking-penetration circle or excitation of 2/1 locked mode is observed due to the changed density or RMP amplitude.

(3) The penetration threshold of 3/1 RMPs scales linearly to the n_e around the 3/1 RS but to $n_e^{0.73}$ for the density at plasma core.

(4) Field penetration of 3/1 RMPs usually causes an increase of ~ 4 km/s for V_ϕ(CV) in the co-I_p direction but little change in V_ϕ(CIII), and V_θ(CV) and V_θ(CIII) is increased for about 1 km/s and 3 km/s towards the ion diamagnetic drift direction.

Reference

[1] Evans T. E. et al 2004 *Physical Review Letters* **92** 235003

[2] Evans T. E. et al 2006 *nature physics* **2** 419

[3] Liang Y. et al 2007 *Physical Review Letters* **98** 265004

[4] Suttrop W. et al 2011 *Physical Review Letters* **106** 225004

[5] Jeon Y. M. et al 2012 *Physical Review Letters* **109** 035004

[6] Kirk A. et al 2013 *Nuclear Fusion* **53** 043007

[7] Jong-Kyu P. et al 2008 *Nuclear Fusion* **48** 045006

[8] Buttery R. J. et al 2012 *Physics of Plasmas* **19** 056111

[9] Paz-Soldan C. et al 2014 *Nuclear Fusion* **54** 073013

[10] Shiraki D. et al 2014 *Nuclear Fusion* **54** 033006

[11] Strait E. J. et al 2014 *Nuclear Fusion* **54** 073004

[12] Kirk A. et al 2014 *Plasma Physics and Controlled Fusion* **56** 104003

[13] In Y. et al 2015 *Nuclear Fusion* **55** 043004

[14] Liu Y. Q. et al 2000 *Physics of Plasmas* **7** 3681

[15] Sabbagh S. A. et al 2006 *Physical Review Letters* **97** 045004

[16] Rath N. et al 2013 *Nuclear Fusion* **53** 073052

[17] Paz-Soldan C. et al 2015 *Nuclear Fusion* **55** 083012

[18] Ryter F. et al 2012 *Nuclear Fusion* **52** 114014

[19] Scannell R. et al 2015 *Plasma Physics and Controlled Fusion* **57** 075013

[20] Mordijck S. et al 2015 *Plasma Physics and Controlled Fusion* **58** 014003

[21] Schmitz O. et al 2009 *Journal of Nuclear Materials* **390-91** 330

[22] Schmitz O. et al 2012 *Nuclear Fusion* **52** 043005

[23] Jakubowski M. W. et al 2013 *Nuclear Fusion* **53** 113012

[24] Evans T. E. et al 1992 *Journal of Nuclear Materials* **196–198** 421

[25] Coenen J. W. et al 2011 *Nuclear Fusion* **51** 063030

[26] Finken K. H. et al 2007 *Physical Review Letters* **98** 065001

[27] Yu Q., Gunter S. 2009 *Nuclear Fusion* **49** 062001

[28] Yu Q., Gunter S. 2011 *Nuclear Fusion* **51** 073030

[29] Tamain P. et al 2010 *Plasma Physics and Controlled Fusion* **52** 075017

[30] Kirk A. et al 2015 *Nuclear Fusion* **55** 043011

[31] Mordijck S. et al 2012 *Physics of Plasmas* **19** 056503

[32] Hu Q. et al 2014 *Nuclear Fusion* **54** 064013

[33] Hu Q. et al 2014 *Nuclear Fusion* **54** 122006

[34] Zhuang G. et al 2011 *Nuclear Fusion* **51** 094020

[35] Rao B. et al 2014 *Fusion Engineering and Design* **89** 378

[36] Chen J. et al 2014 *Review of Scientific Instruments* **85** 11D303

[37] Ding Y. H. et al 2014 *Review of Scientific Instruments* **85** 043502

[38] Yang Z. J. et al 2012 *Review of Scientific Instruments* **83** 10E313

[39] Cheng Z. F. et al 2013 *Review of Scientific Instruments* **84** 073508

[40] Hender T. C. et al 1992 *Nuclear Fusion* **32** 2091

[41] Hu Q. et al 2012 *Nuclear Fusion* **52** 083011

[42] Hu Q. et al 2013 *Physics of Plasmas* **20** 092502

[43] Frassinetti L. et al 2014 *Plasma Physics and Controlled Fusion* **56** 104001

[44] Schmitz O. et al 2014 *Nuclear Fusion* **54** 012001

[45] Buttery R. J. et al 1999 *Nuclear Fusion* **39** 1827

[46] Buttery R. J. et al 2000 *Nuclear Fusion* **40** 807

[47] Howell D. F. et al 2007 *Nuclear Fusion* **47** 1336

[48] Loewenbrueck K. et al 2007 *34th EPS Conference on Plasma Phys (Warsaw, Poland, 2007)* vol 31F (ECA), p -1.136 http://epsppd.epfl.ch/Warsaw/pdf/P1_136.pdf

[49] Wang N. et al 2014 *Nuclear Fusion* **54** 064014

[50] Jin H. et al 2015 *Plasma Physics and Controlled Fusion* **57** 104007

[51] Schmitz O. et al 2008 *Nuclear Fusion* **48** 024009

[52] Xu Y. et al 2006 *Physical Review Letters* **97** 165003

[53] Xu Y. et al 2007 *Nuclear Fusion* **47** 1696

[54] Mordijck S. et al 2012 *Physics of Plasmas* **19** 024504

[55] Yu Q., et al 2009 *Physics of Plasmas* **16** 042301